

# Creation of multiple nanodots by single ions

September 13, 2018

<sup>1</sup>Ender Akcöltekin, <sup>1</sup>Thorsten Peters, <sup>1</sup>Ralf Meyer, <sup>1</sup>Andreas Duvenbeck, <sup>1</sup>Miriam Klusmann,

<sup>2</sup>Isabelle Monnet, <sup>2</sup>Henning Lebius, <sup>1</sup>Marika Schleberger\*

<sup>1</sup> *Universität Duisburg-Essen, FB Physik, 47048 Duisburg, Germany*

<sup>2</sup> *CIRIL (CEA, CNRS, ENSICAEN), 14070 Caen Cedex 5, France*

**In the challenging search for tools that are able to modify surfaces on the nanometer scale, heavy ions with energies of several 10 MeV are becoming more and more attractive. In contrast to slow ions where nuclear stopping is important and the energy is dissipated into a large volume in the crystal, in the high energy regime the stopping is due to electronic excitations only [1, 2, 3]. Because of the extremely local ( $\leq 1$  nm) energy deposition with densities of up to  $10^{19}$  W/cm<sup>2</sup>, nanoscaled hillocks can be created under normal incidence [4, 5, 6]. Usually, each nanodot is due to the impact of a single ion and the dots are randomly distributed. We demonstrate that multiple periodically spaced dots separated by a few 10 nanometers can be created by a single ion if the sample is irradiated under grazing angles of incidence. By varying this angle the number of dots can be controlled.**

As samples we used strontium titanate ( $\text{SrTiO}_3$ ) single crystals, a model substance for the class of perovskites ( $\text{ABO}_3$ ). The ferroelectric oxide  $\text{SrTiO}_3$  is of use in a wide variety of applications:  $\text{SrTiO}_3$  is used in catalysis [7] and is discussed as a possible material for nuclear waste management [8].  $\text{SrTiO}_3$  is the insulator of choice for the fabrication of future microelectronic devices. Because of its high dielectric constant thin films of  $\text{SrTiO}_3$  have only a very low tunneling current compared

---

\*Corresponding author: marika.schleberger@uni-due.de

to conventionally used  $\text{SiO}_2$  [9, 10]. In addition, it is widely used as substrate material for GaAs solar cells and for the deposition of high-temperature superconductors. For the latter, patterning of the substrate is known to influence the critical current densities [11]. Therefore, the creation of regular nanometer sized structures in  $\text{SrTiO}_3$  might as well proof useful for technological applications.

After irradiation under grazing angles of a few degrees with respect to the surface plane (see fig. 4) the samples were imaged by atomic force microscopy (AFM) *in situ* under ultra high vacuum (UHV) conditions. In fig. 1 we show an AFM image of a sample that was irradiated under two different incidence angles, resulting in two different types of defects. If irradiated at  $\Theta = 6^\circ$ , slightly elongated hillocks occur. If the angle is changed to  $\Theta = 3^\circ$ , round almost evenly spaced hillocks appear which are still overlapping. At angles smaller than  $\Theta = 3^\circ$  the dots are clearly separated and the tracks look like pearls on a chain as can be seen in fig. 2 (this sample was irradiated at  $\Theta = 1^\circ$  and at  $\Theta = 2^\circ$ ). The number of chains corresponds to the number of ions. This means each chain containing dozens of nanodots is created by a single ion traveling through the solid. From analyzing more than 600 individual chains irradiated under different angles  $\Theta$  we find that the length  $l$  of the chains can be controlled by varying the angle of incidence as can be seen in fig. 3. At  $\Theta = 1^\circ$  most of the chains are already about half a micron in length. The average height value we find for all chains stemming from irradiations at incidence angles of less than  $3^\circ$  is  $(2.5 \pm 1.0)$  nm. They are of circular shape with a diameter (FWHM) of  $(25 \pm 5)$  nm. The distance between individual hillocks depends on the angle of incidence and is e.g.  $(35 \pm 3)$  nm for the marked chain in fig. 2. Similar measurements (not shown here) on irradiated  $\text{TiO}_2$  and  $\text{Al}_2\text{O}_3$  show the same chains of dots as on  $\text{SrTiO}_3$ . We take this as an indication that this phenomenon may be typical not only for perovskites but also for other oxidic materials.

To date, the patterning of ferroelectric oxides has been achieved by self-organizing ('bottom-up') approaches [12, 13] as well as by 'top-down' methods such as lithography using low energy ions [14], evaporation through a shadow mask [15] or a combination of both [16]. With these techniques the created structures are either randomly distributed or shaped, or the periodicity is limited to 100 nm at best. To our knowledge, no other technique that is able to create regular shaped nanodots on a perovskite surface with a spacing of 35 nm has so far been established.

In order to describe the ion-solid interaction the so-called thermal spike (TS)-model has been

developed [17]. Toulemonde *et al.* applied it to the special case of swift heavy ions where electronic stopping dominates over nuclear stopping by orders of magnitude [18]. It describes the formation of cylindrical tracks of amorphous or recrystallized material inside the solid. It does neither explain the formation mechanism of hillocks on the surface nor the formation of hillock chains. The starting point to gain an understanding of the formation of nanodot chains on  $\text{SrTiO}_3$  are early experiments with van der Waals materials such as  $\text{MoS}_2$  or  $\text{WSe}_2$ . In these materials intermittent fission tracks were observed by transmission electron microscopy [19]. These discontinuous tracks were explained by the strong spatial anisotropy of a van der Waals crystal lattice. The  $\pi$ -electrons are fully contained within the crystal planes and there is only a weak hydrogen bond between the planes. Each time the projectile hits a lattice plane with a high density of electrons, enhanced electronic stopping occurs. This significant anisotropy leads to periodic spikes of radiation damage in this type of materials as observed by Morgan and Chadderton [19]. Such a triggered loss process could also explain the distinct features we observe.

If the ion travels through  $\text{SrTiO}_3$  it will continuously interact with the electronic system of the material but energy loss is more probable where the electron density is high. There, the sudden interaction of the projectile with the electronic system gives rise to a sharply peaked energy distribution. How this electronic excitation finally leads to the modification of the material (craters, hillocks, tracks, etc.) is still not exactly known. The thermal spike model describes the energy transport out of the electronically heated region, whereas the Coulomb explosion model [20] couples the electronic excitation to atomic motion caused by the repulsive forces acting in the transiently ionized region. Both models cover important aspects of the creation processes for material modifications [21]. In our experiment the strong ionization rate of the swift heavy ion leads to a significant charge imbalance. From Shimas empirical formula [22] and extrapolating experimental data [23], respectively, we find that Xe ions moving through  $\text{SrTiO}_3$  with 92 MeV have an effective equilibrium charge close to the original charge state of  $q_{\text{eff}}=23$ . However, our data does not allow us to make a clear correlation with neither of the two scenarios. In any case, for both models to be predictive the initial conditions need to be known. A strong anisotropy of the electronic structure as e.g. in a van der Waals material will influence the loss process significantly, be it connected either to a Coulomb explosion or to a thermal spike.

Note however, that  $\text{SrTiO}_3$  is not a van der Waals material and the observed features cannot be simply attributed to the ion crossing crystal layers of a homogeneous electron density. If the anisotropy was exclusively parallel to the surface (as is the case with  $\text{MoS}_2$ ), we would observe that the number of nanodots was constant and the distance between dots would vary as a function of the angle of incidence. If the anisotropy was exclusively normal to the surface, we would observe a varying number of dots, but the distance between them would be constant. In our case the anisotropy is given parallel as well as normal to the surface. Therefore, the observed distance between dots and the number of the dots as a result of a triggered loss process needs to be discussed taking the full three dimensional electronic structure into account. To this end, we performed *ab-initio* density functional theory (DFT) calculations to determine the electronic density of  $\text{SrTiO}_3$  and projected the density onto the plane of the traveling ion (see fig. 5).

Most of the electrons are located around the oxygen atoms and the density is higher in the  $\text{TiO}_2$  planes than in the  $\text{SrO}$  planes (see fig. 4). Simple geometrical considerations taking the electron density into account yield a very good qualitative agreement with the periodic defects occurring in  $\text{SrTiO}_3$  as can be seen from fig. 5. In this approach we have used the DFT data to calculate the electron density encountered by an ion following a typical trajectory (azimuthal angle  $\varphi = 0^\circ$ , see fig. 4) through a perfect  $\text{SrTiO}_3$  crystal under a grazing angle of  $\Theta = 0.5^\circ$ . On its way through a single lattice plane the ion interacts with the electrons of several dozens of oxygen atoms. Each peak in the fine structure (see upper panel in fig. 5) is due to the interaction of the ion with the electrons surrounding one oxygen atom. The sum of these interactions within one crystal plane (large peaks in the lower panel of fig. 5) creates a strong local excitation leading finally to a nanodot on the surface. The ion then typically travels several hundred Ångström through the crystal without energy loss before it again encounters an area with a high enough electron density.

Even though the exact mechanisms of the observed dot formation (fig. 1 and fig. 2) are not known, we may assume the space- and time dependent *generation* of excitation energy  $E_s(\vec{r}, t)$  along the trajectory of the projectile  $\vec{r}_p(t)$  as well as the *transport* of excitation energy to play a key role in that process. In the energy regime considered here, the generation of excitation energy can be approximately treated within the frame of the Lindhard model [24] of electronic stopping. Employing that framework, the excitation energy  $dE_s(\vec{r}_p(t))$  that is transferred from the kinetic energy of the

projectile into the electronic system within the time interval  $dt$  is proportional to the momentary kinetic energy of the projectile and - even more important in our context - to the local electron density  $n_{el}(\vec{r}_p(t))$  provided by the ab-initio DFT calculations as explained above. We assume the time evolution of the four-dimensional profile  $E(\vec{r}, t)$  of excitation energy within the solid to be described by the diffusion equation

$$\frac{\partial E}{\partial t}(\vec{r}, t) - D \nabla^2 E(\vec{r}, t) = \frac{dE_s}{dt}(\vec{r}_p(t), E_{kin}(\vec{r}_p(t)), n_{el}(\vec{r}_p(t))) \quad (1)$$

with  $D$  denoting the diffusion coefficient. The projectile trajectory  $\vec{r}_p(t)$  entering Eq. (1) is obtained by numerically integrating the Newtonian equations of motion including an effective friction term originating from the Lindhard treatment. In view of the fact that on the one hand the lateral dimensions of the observed nanodots are of the order of several tens of nanometers, but, on the other hand, the electron density within one unit cell varies on the sub-Ångström length-scale, a straight-forward numerical treatment of Eq. (1) is hampered by the complexity of the problem.

It should be emphasized here that in our case (i) the consideration of the local electron density on a sub-Ångström length scale and (ii) the necessity for the correct incorporation of the surface plane into the excitation energy transport process principally disallows the reduction of the problem to radial symmetry with respect to the swift heavy ion track as usually done in (TS)-model calculations [25]. In contrast to the (TS)-model calculations, we propose to perform a nested two-step calculation approach as follows: In the first step, we take advantage of the straightness of the ion track and - for given impact parameters  $(\Theta, \phi)$  - geometrically determine the set of intersection points through the unit cells along the trajectory of the projectile. This procedure is performed for a total trajectory length  $L$  which corresponds to a laterally projected range larger than the observed period length of the nanodots. Starting from the unit cell at the impact point, each traversed cell is discretized into more than  $10^5$  voxels to match the sub-Ångström resolution of  $n_{el}(\vec{r}, t)$ . A numerical integration of the equations of motion of the projectile employing the highly-resolved electron density yields the total generated excitation energy  $dE_s(\vec{r}_p(t))$  as well as the traveling time  $dt$  for that cell. Naturally, the kinetic energy of the heavy ion is reduced after traversing one cell due to electronic stopping.

This reduced energy as well as the exit point of one cell are taken as the new initial parameters for the analogous calculation carried out for the subsequent cell. Iteration of this algorithm yields a set

of  $(dE/dt)_i$  which in the second step of our model, are treated as distinct point sources of excitation energy in a discrete representation of Eq. (1) with a grid-spacing in units of one elementary cell. Using that coarse discretization the numerical solution of Eq. (1) can be obtained via a Green's functions approach for the half space diffusion problem.

In the present study we focus our interest on the striking periodicity of the nanodots which should already be present in the space dependence of the electronic stopping (ES)  $dE_s/dx$  along the trajectory derived from  $\frac{dE_s}{dt}(\vec{r}_p(t))$  of Eq. (1). Fig. 6 shows the result of an exemplary calculation of this ES for a 0.711 MeV/u Xe projectile hitting a SrTiO<sub>3</sub> crystal under  $\Theta = 0.5^\circ$  and  $\phi = 10^\circ$ . Two kinds of peaks can be seen, one originating from the TiO<sub>2</sub> planes, the second one from the SrO planes. The average ES in the TiO<sub>2</sub> planes is higher by a factor of 2 (integrating over the peak area). Thus, for this particular choice of impact parameters, the periodicity of the dot formation may be governed by the contribution of the TiO<sub>2</sub> planes. The decrease of the maximum peak heights with increasing track length  $L$  due to electronic friction will be one factor limiting the total chain length  $l$ . A more quantitative discussion of features such as e.g. chain length, track radius and temporal dynamics goes beyond the scope of this paper because it would require a detailed analysis of the full four-dimensional excitation energy profile  $E(\vec{r}, t)$  obtained from Eq. (1) using the ES discussed above.

Our model is further corroborated by plotting the measured length of the chains as a function of the angle of incidence as shown in fig. 3. The data can be fitted nicely by using  $l(\Theta) = d/(\tan\Theta)$ . Here,  $l$  is the length of the chain, and  $d$  is the maximum depth from where the excitation starts (see inset in fig. 3). In addition, we frequently observe, that at the very end of a chain the height of the dots decreases monotonic. These findings could be explained if we assume that the ion is traveling already too deep below the surface and the material modifications do not reach the surface any longer. In this way, we can determine the radius of the modified volume from our data. Our value of ca. 10 nm is larger by a factor of 2 than the effective latent track radii derived from irradiation experiments on different insulators under 90°[26, 27]. Repeating our experiment with an amorphous layer of SiO<sub>2</sub>, we find periodic dots as well [28]. It is not clear yet, what the origin of this periodicity is, but it could be the electron density, maybe even of the underlying crystalline Si substrate.

In conclusion, we have demonstrated how to produce periodic nanodots on oxidic surfaces by a single ion hit. We propose that the anisotropic electron density of the material gives rise to a triggered

energy loss process. The resulting nanodots imaged by AFM thus represent a direct view of the projection of the three-dimensional electronic density onto the surface.

## Methods

### Experimental setup, sample preparation and image processing

The experiments were performed at the beamline IRRSUD of the Grand Accelerateur National d’Ions Lourds (GANIL) in Caen, France. An UHV-AFM/STM (Omicron Nanotechnology, Taunusstein) was mounted directly to the chamber where the irradiation with swift heavy ions took place. The base pressure was  $2 \times 10^{-8}$  mbar in the differentially pumped irradiation chamber and  $1 \times 10^{-10}$  mbar in the AFM. As samples we used commercially available  $\text{SrTiO}_3(100)$ ,  $\text{TiO}_2(100)$  and  $\text{Al}_2\text{O}_3(1102)$  crystals (CrysTec, Berlin). The samples were cleaned with acetone. We did not use any etching to get rid of excess  $\text{SrO}$  terminations since this would not play a role in the hillock formation. AFM images taken before irradiation to check the cleanliness of the samples frequently showed atomically flat terraces separated by atomic steps.

The samples were irradiated with a beam of  $\text{Xe}^{23+}$  ions at 0.711 MeV/u scanned over the whole surface area of the target. Typically, a fluence of  $1 \times 10^9$  ions/cm<sup>2</sup> was chosen resulting in 10 impacts per  $\mu\text{m}^2$  on average. At this fluence enough events are produced to obtain a good statistic but the probability that two ions hit the same spot resulting in non-linear phenomena is still sufficiently low. For  $\text{SrTiO}_3$  the chosen projectile/energy combination results in an energy loss of 19.1 keV/nm as calculated with SRIM [29]. The angle of incidence with respect to the surface was varied between  $\Theta=1^\circ$  and  $\Theta=6^\circ$ . Due to the experimental setup the uncertainty of the absolute angle is not better than  $\pm 1^\circ$ . Due to technical limitations the azimuthal angle  $\varphi$  was not controlled in our experiment. Immediately after irradiation all samples were measured with the AFM using the contact ( $F = 0.2$  nN) as well as the dynamic (non-contact) mode ( $df = -10$  Hz) *in situ*. Additional data from *ex-situ* measurements was used for fig. 3. No chemical etching or post-irradiation treatment was applied. This ensures that all observed topographical features can be attributed unambiguously to the irradiation.

All AFM images were recorded with the Omicron SCALA software version 4.1 and processed with the Nanotec Electronica SL WSxM software, version 4.0 Develop 8.3. From the raw data ( $400 \times 400$  data points) only a plane was subtracted. The colour code was changed using the palette *flow.lut*. No change of contrast (1) or brightness (0) was used.

### DFT calculations

The density functional theory (DFT) calculations were performed using the ABINIT package [30] together with pseudopotentials generated by the fhi98pp code [31] in order to determine the distribution of the electrons in  $\text{SrTiO}_3$ . For the exchange-correlation energy the Perdew-Burke-Ernzerhof generalized-gradient approximation functional [32] was used. In a first step, the equilibrium lattice constant of the investigated system was obtained.

The result is  $7.53\text{ }a_{\text{B}}$  for  $\text{SrTiO}_3$ . Subsequently the electron density at the equilibrium lattice constant was derived. A common kinetic-energy cutoff-energy of 96 Hartree for the expansion of the wave functions and a  $8 \times 8 \times 8$  k-point mesh were used in all calculations.

## Acknowledgement

Financial support by the DFG - SFB616: *Energy dissipation at surfaces* and SFB 445: *Nanoparticles from the Gas Phase*, by the GANIL (Project S18) and by the European Community FP6 - Structuring the ERA - Integrated Infrastructure Initiative-contract EURONS n° RII-CT-2004-506065 is gratefully acknowledged. We thank Philippe and Frederic JeanJean for their help with the experiment and Andreas Reichert for valuable discussions.

## References

- [1] H.A. Bethe. Zur Theorie des Durchgangs schneller Korpuskularstrahlen durch Materie. *Ann. Phys.*, 397:325, 1930.
- [2] F. Bloch. Zur Bremsung rasch bewegter Teilchen beim Durchgang durch Materie. *Ann. Phys.*, 408:285, 1933.
- [3] J. Lindhard, M. Scharff, and H.E. Schiøtt. Range concepts and heavy ion ranges (Notes on atomic collisions II). *Kgl. Dansk Videnskab. Selskab. Mat.-Fys. Medd.*, 33:14, 1963.
- [4] R. Neumann. Scanning probe microscopy of ion-irradiated materials. *Nucl. Instr. Meth. B*, 151:42, 1999.
- [5] S. Bouffard, J. Cousty, Y. Pennec, and F. Thibaudau. STM and AFM observations of latent tracks. *Radiat. Eff. Defects Solids*, 126:225, 1993.
- [6] N. Khalfaoui, M. Görlich, C. Müller, M. Schleberger, and H. Lebius. Latent tracks in CaF<sub>2</sub> studied with atomic force microscopy in air and in vacuum. *Nucl. Instr. Methods B*, 245:246, 2006.
- [7] R. Li, Q. Tang, S. Yin, and T. Sato. Plasma catalysis for CO<sub>2</sub> decomposition by using different dielectric materials. *Fuel Processing Technol.*, 87:617, 2006.
- [8] S. Thevuthasan, V. Shuthanandan, and Y. Zhang. Applications of high energy ion beam techniques in environmental science: Investigation associated with glass and ceramic waste forms. *J. Electr. Spectr. Rel. Phen.*, 150:195, 2006.
- [9] S. Jeon, F.J. Walker, C.A. Billman, R.A. McKee, and H. Hwang. Electrical Characteristics of Epitaxially Grown SrTiO<sub>3</sub> on Silicon for Metal-Insulator-Semiconductor Gate Dielectric Applications. *IEEE Electron Device Letters*, 24:218, 2003.
- [10] C.J. Först, C.R. Ashman, K. Schwarz, and P.E. Blöchl. The interface between silicon and a high-*k* oxide. *Letters to Nature*, 427:53, 2004.

[11] S. Brück and J. Albrecht. Experimental evidence of the dominant role of low-angle grain boundaries for the critical current density in epitaxially grown  $\text{YBa}_2\text{Cu}_3\text{O}_{7-\delta}$  thin films. *Phys. Rev. B*, 71:174508, 2005.

[12] M. Zhang, X.L. Ma, D.X. Li, H.B. Lu, Z.H. Chen, and G.Z. Yang. Patterned nanoclusters in the indium-doped  $\text{SrTiO}_3$  films. *Appl. Phys. Lett.*, 85:5899, 2004.

[13] I. Szafraniak, C. Harnagea, R. Scholz, S. Bhattacharyya, D. Hesse, and M. Alexe. Ferroelectric epitaxial nanocrystals obtained by a self-patterning method. *Appl. Phys. Lett.*, 83:2211, 2003.

[14] J. Albrecht, S. Leonhardt, R. Spolenak, U. Täffner, H.-U. Habermeier, and G. Schütz. Surface patterning of  $\text{SrTiO}_3$  by 30 keV ion irradiation. *Surf. Sci.*, 547:L847, 2003.

[15] H.-J. Shin, J.H. Choi, H.J. Yand, Y.D. Park, Y. Kuk, and C.-J. Kang. Patterning of ferroelectric nanodot arrays using a silicon nitride shadow mask. *Appl. Phys. Lett.*, 87:113114, 2005.

[16] D. Ruzmetov, Y. Seo, L.J. Belenky, D.M. Kim, X. Ke, H. Sun, V. Chandrasekhar, C.B. Eom, M.S. Rzchowski, and X. Pan. Epitaxial Magnetic Perovskite Nanostructures. *Advanced Materials*, 17:2869, 2005.

[17] F. Seitz and J.S. Köhler. Displacement of Atoms during Irradiation. *Solid State Physics: Advances in Research and Applications*, Eds. F. Seitz and D. Turnbull, 2:305–448, 1956.

[18] M. Toulemonde, C. Dufour, and E. Paumier. Transient thermal process after a high-energy heavy-ion irradiation of amorphous metals and semiconductors. *Phys. Rev. B*, 46:14362, 1992.

[19] D.V. Morgan and L.T. Chadderton. Fission Fragment Tracks in Semiconducting Layer Structures. *Phil. Mag.*, 17:1135, 1968.

[20] R.L. Fleischer, P.B. Price, and R.M. Walker. Ion Explosion Spike Mechanism for Formation of Charged-Particle Tracks in Solids. *J. Appl. Phys.*, 36:3645, 1965.

[21] S. Klaumünzer. Ion tracks in quartz and vitreous silica. *Nucl. Instr. Methods B*, 225:136, 2004.

[22] K. Shima, T. Ishihara, T. Miyoshi, and T. Mikumo. Equilibrium charge-state distributions of 35–146-MeV Cu ions behind carbon foils. *Phys. Rev. A*, 28:2162, 1983.

- [23] K. Shima, N. Kuno, and M. Yamanouchi. Systematics of equilibrium charge state distributions of ions passing through a carbon foil over the ranges  $Z=4\text{--}92$  and  $E=0.02\text{--}6$  MeV/u. *Phys. Rev. A*, 40:3557, 1989.
- [24] J. Lindhard and M. Scharff. Energy Dissipation by Ions in the kev Region. *Phys. Rev.*, 124:128, 1961.
- [25] M. Toulemonde, C. Dufour, and E. Paumier. The Ion-Matter Interaction with Swift Heavy Ions in the Light of Inelastic Thermal Spike Model. *Acta Physica Polonica A*, 109:311, 2006.
- [26] A. Meftah, F. Brisard, J.M. Costantini, E. Dooryhee, M. Hage-Ali, M. Hervieu, J.P. Stoquert, F. Studer, and M. Toulemonde. Track formation in  $\text{SiO}_2$  quartz and the thermal-spike mechanism. *Phys. Rev. B*, 49:12457, 1994.
- [27] G. Szenes. General features of latent track formation in magnetic insulators irradiated with swift heavy ions. *Phys. Rev. B*, 51:8026, 1995.
- [28] A.M.J.F. Carvalho, M. Marinoni, A.D. Touboul, C. Guasch, H. Lebius, M. Ramonda, J. Bonnet, and F. Saigne. Discontinuous ion tracks on silicon oxide on silicon surfaces after grazing angle heavy ion irradiation. *Appl. Phys. Lett.*, accepted, 2007.
- [29] J.F. Ziegler and J.P. Biersack. The stopping and range of ions in matter. URL <http://www.SRIM.org>, Version 2003.26.
- [30] The abinit code is a common project of the Université Catholique de Louvain, Corning Incorporated, and other contributors. URL <http://www.abinit.org>.
- [31] M. Fuchs and M. Scheffler. Ab initio pseudopotentials for electronic structure calculations of poly-atomic systems using density-functional theory. *Comput. Phys. Commun.*, 119:67, 1999.
- [32] J.P. Perdew, K. Burke, and M. Ernzerhof. Generalized Gradient Approximation Made Simple. *Phys. Rev. Lett.*, 77:3865, 1996.

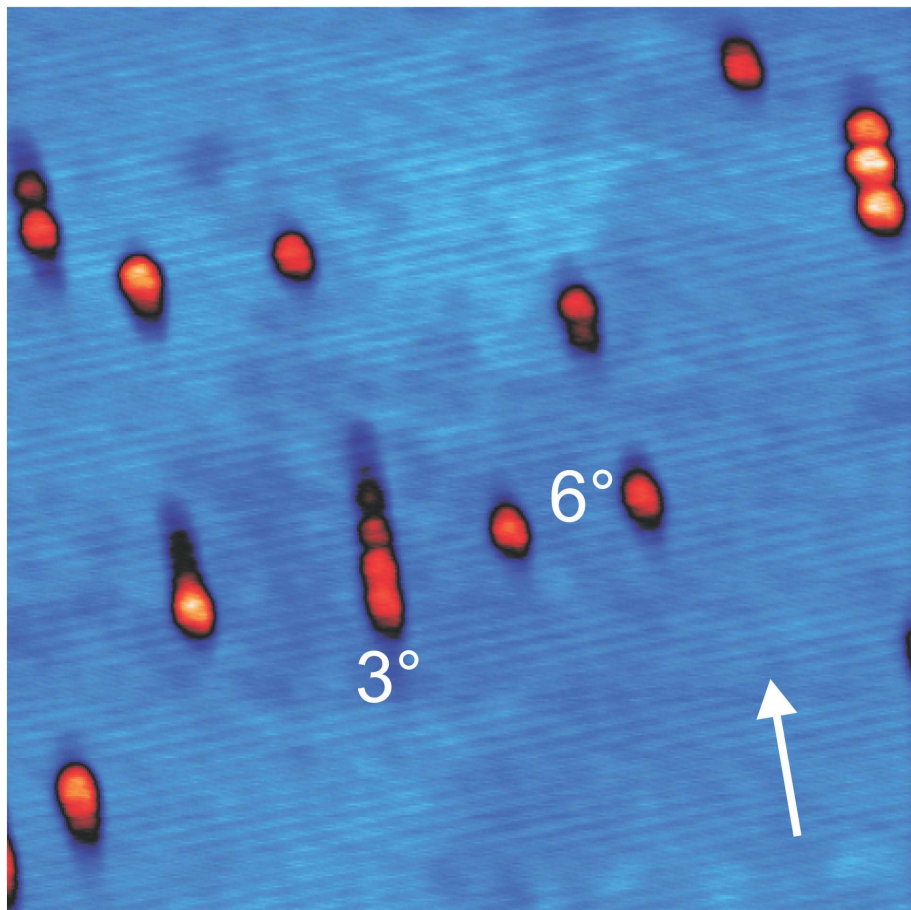


Figure 1: Typical nanodots on  $\text{SrTiO}_3$  created by irradiation with 92 MeV Xe ions. Frame size 500 x 500 nm<sup>2</sup>, colour scale from 0 to 4.4 nm. The sample was irradiated two times. The angle of incidence was  $\Theta = 3^\circ$  and  $\Theta = 6^\circ$ , respectively. Each dot or chain, respectively, corresponds to a single ion hit. To enhance the contrast false colouring was used. The arrow indicates the direction of the incoming ions.

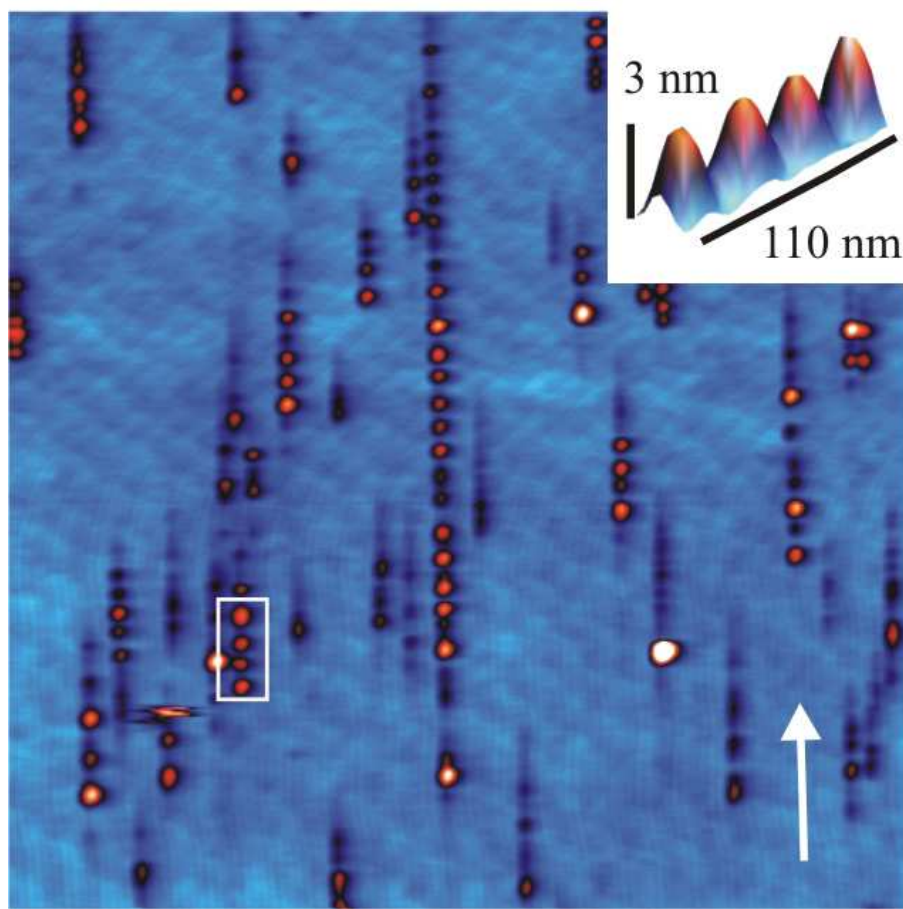


Figure 2: Typical chains of nanodots on  $\text{SrTiO}_3$  created by irradiation with 92 MeV Xe ions. Frame size  $1300 \times 1300 \text{ nm}^2$ , colour scale from 0 to 3.7 nm. The sample was irradiated two times. The angle of incidence was  $\Theta = 1^\circ$  and  $\Theta = 2^\circ$ , respectively. The inset shows size and shape of the individual dots within a chain.

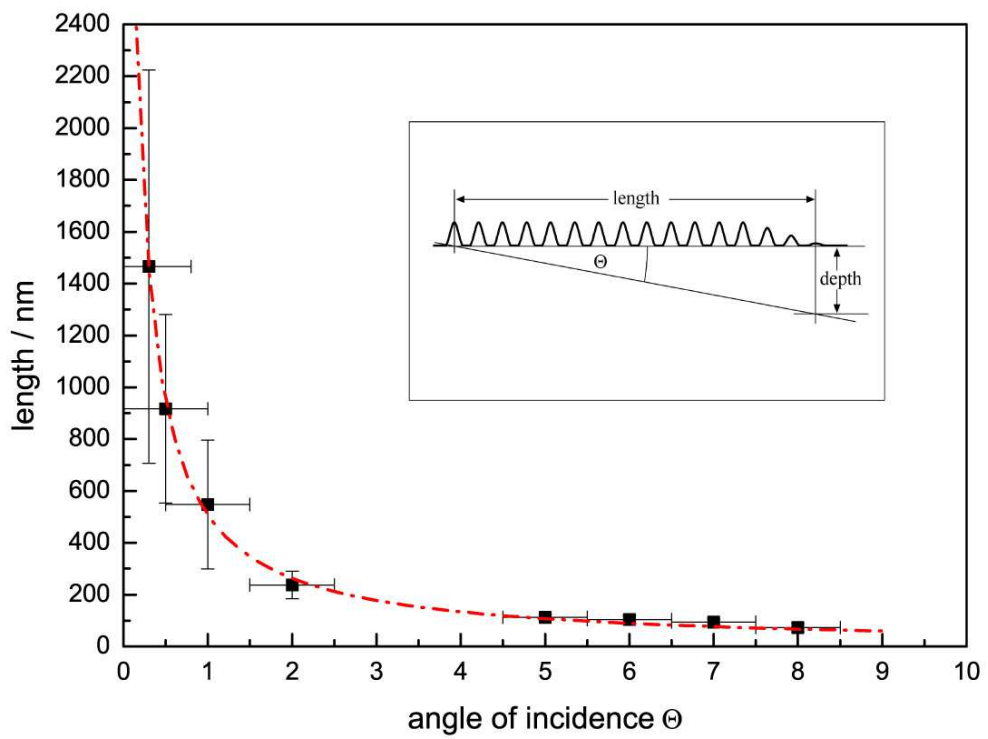


Figure 3: Measured length  $l$  of chains as a function of angle of incidence. The dash-dotted line is a fit according to our model with  $d = 9.8$  nm (see text).

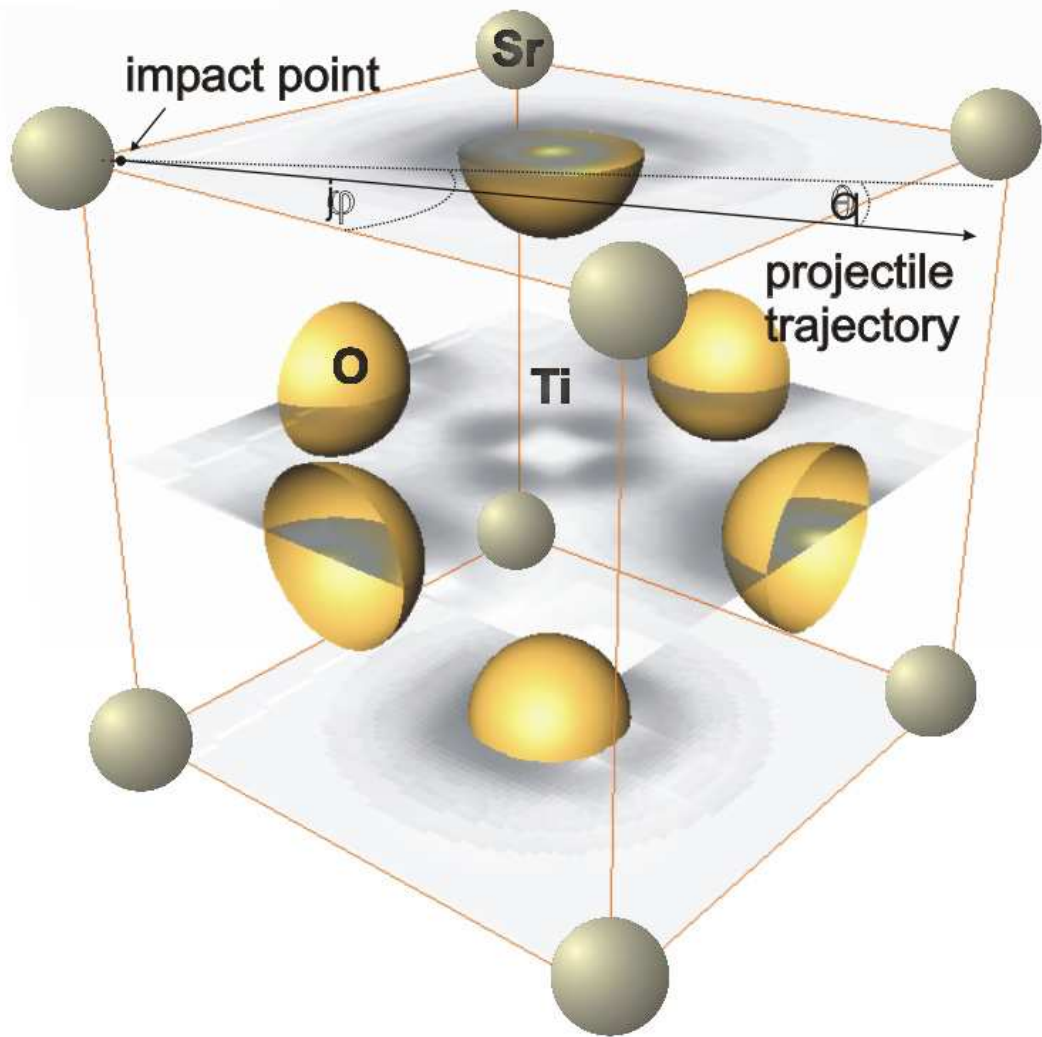


Figure 4: DFT calculation of the electron density (gray shading) of SrTiO<sub>3</sub>. Atom positions (besides the central titanium atom) are also visualized. The arrow indicates a possible projectile trajectory.

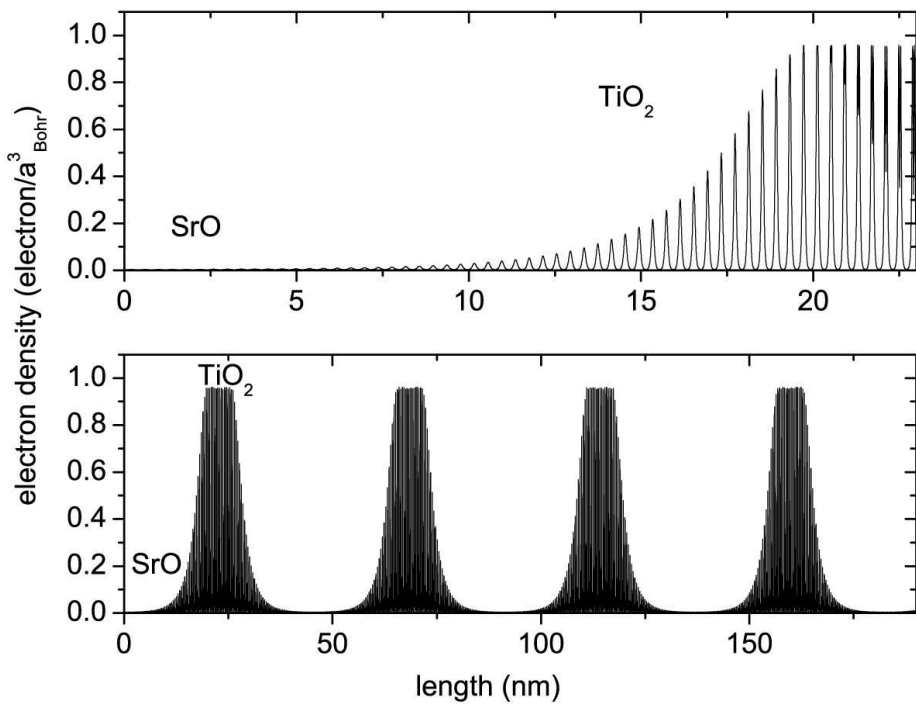


Figure 5: Simulation of the electron density which the ion encounters when traveling through the crystal lattice at a grazing angle of  $\Theta = 0.5^\circ$  with respect to the (100)-surface plane of a SrTiO<sub>3</sub> single crystal (see fig. 4).

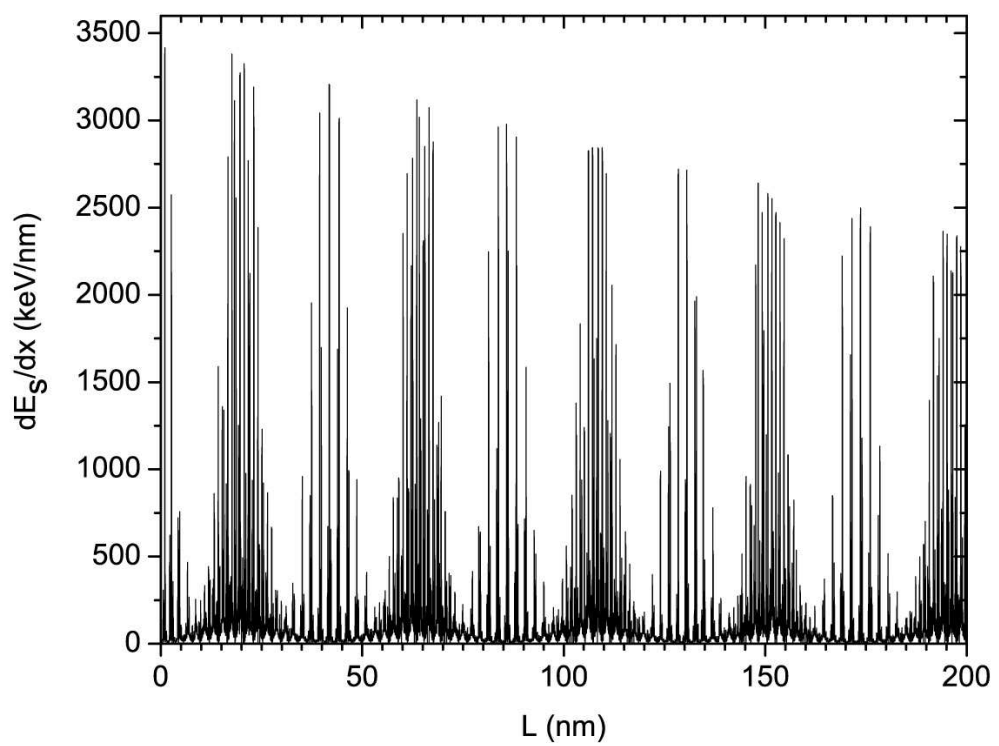


Figure 6: Electronic stopping  $dE_s/dx$  along the track of a Xe projectile hitting a  $\text{SrTiO}_3$  single crystal with  $\Theta = 0.5^\circ$  and  $\phi = 10^\circ$ .